

High thermoelectric performance in two-dimensional tellurium: An *ab initio* study

Zhibin Gao,[†] Gang Liu,^{*,‡} and Jie Ren^{*,†}

[†]Center for Phononics and Thermal Energy Science, China-EU Joint Center for Nanophononics, Shanghai Key Laboratory of Special Artificial Microstructure Materials and Technology, School of Physics Sciences and Engineering, Tongji University, Shanghai 200092, China

[‡]School of Physics and Engineering, Henan University of Science and Technology, Luoyang 471023, China

E-mail: liugang8105@gmail.com; Xonics@tongji.edu.cn

Abstract

In 2016, bulk tellurium was experimentally observed as a remarkable thermoelectric material. Recently, two-dimensional (2D) tellurium, called tellurene, has been synthesized and has exhibited unexpected electronic properties compared with the 2D MoS₂. They have also been fabricated into air-stable and high efficient field-effect transistors. There are two stable 2D tellurene phases. One (β -Te) has been confirmed with an ultralow lattice thermal conductivity (κ_L). However, the study of the transport properties of the other more stable phase, α -Te, is still lacking. Here, we report the thermoelectric performance and phonon properties of α -Te using Boltzmann transport theory and first principle calculations. A maximum ZT value of 0.83 is achieved under reasonable hole concentration, suggesting that the monolayer α -Te is a potential competitor in the thermoelectric field.

Keywords

tellurene, stability, Seebeck coefficient, strong anharmonicity, thermoelectric material

1 Introduction

Recently, 2D materials have triggered a large number of interest due to the striking physical properties related to the low dimensionality.¹⁻³ Graphene¹ in group-IV, borophene in group-III^{4,5} and black phosphorous in group-V^{6,7} have been extensively investigated experimentally and theoretically. However, researches related to group-VI monolayer materials are still lacking to date.

Recently, Zhu *et al.*⁸ firstly have proposed three novel types of monolayer tellurene, namely α -, β - and γ -Te. Afterwards, tellurene has been synthesized and attracted lots of interest.⁸⁻¹⁵ These findings indicate that tellurene possesses unusually physical properties, especially for applications in electronic and thermoelectric devices. Furthermore, Wang *et al.*¹⁰ pointed out that tellurene can be obtained in a very large scale and can be fabricated into air-stable and high-performance field-effect transistors, which makes it different from other 2D materials. Furthermore, tellurene has much larger carrier mobility than that of 2D MoS₂.⁸ Few layer tellurene also has extraordinarily electronic transport properties.^{10,14,15}

β -Te has the intrinsic κ_L of 2.16 and 4.08 W/mK along both directions (300 K)¹² and also shows significant anisotropy, indicating good potential in application of thermoelectric devices with $ZT = 0.8$.¹⁶ Besides, in 2016, bulk tellurium was experimentally observed as a remarkable thermo-

electric material.¹⁷ Energetically, monolayer α -Te is the most stable structure compared with the metastable β - and γ -Te phases.⁸ As the most stable phase, α -Te is also a promising one to be synthesized experimentally and has applications in practical nanoelectronics.

Generally, we use ZT to assess the degree of thermoelectric material by $ZT = S^2\sigma T/(\kappa_e + \kappa_L)$, where S means Seebeck coefficient, σ is the electric conductivity, T is the absolute temperature, κ_e and κ_L are the electronic and lattice thermal conductivity, respectively. Ideally, one would like to enhance the numerator and weaken the denominator at the same time. Fortunately, one can enhance the scattering of phonons by boundary, defect, isotopic effect, resonant bonding,¹⁸ rattle-like scattering,¹⁹ lone electron pairs,²⁰ making composite structures²¹ and even forming solid solutions.²² Unfortunately, S and σ unusually interweave and behave in an opposite trend, which induces the complexity to efficiently realize the waste heat recovery.²¹

Interestingly, low dimensional such as 2D materials have the potential to break above relation between S and σ due to the quantum confinement effect pointed by Dresselhaus *et al.*³ There are three phases of atomically thin tellurium, namely α -, β - and γ -Te. The first two are energetically, dynamically and mechanically stable. Furthermore, α -Te is more stable than β -Te⁸ that has an unusually low κ_L ¹² and superior thermoelectric property.¹⁶ However, relevant works about κ_L and thermoelectric properties of the more stable α -Te phase is still lacking. In this letter, we focus on the more stable phase, α -Te, and would like to explore its novel electronic and thermal properties. We find a largest ZT (0.83) is achieved under reasonable hole concentration at 700 K for α -Te.

2 Computational methods

We use vasp code and PBE functional.^{23–25} The cutoff energy is 500 eV. In order to obtain a more accurate electronic band structure and density of states, we use HSE06 approach.²⁶ The van der Waals (vdW) correction proposed by Grimme²⁷ was taken into consideration in our calculations. The criterion of convergence energy and force are

10^{-6} eV and $1 \text{ meV}/\text{\AA}$. We use $17 \times 17 \times 1$ k-mesh in the Brillouin zone.

In the framework of Boltzmann transport theory (BTE), the electrical transport properties, such as σ , S and κ_e can be expressed as:^{28,29}

$$\mathbf{K}_n = \frac{1}{4\pi^3} \sum_{i,\mathbf{k}} \tau_i(\mathbf{k}) \mathbf{v}_i(\mathbf{k}) \otimes \mathbf{v}_i(\mathbf{k}) [\varepsilon_i(\mathbf{k}) - \mu]^n \times \left[-\frac{\partial f(\mu, T, \varepsilon_i)}{\partial \varepsilon_i} \right], \quad (1)$$

$$\sigma = e^2 \mathbf{K}_0, \quad (2)$$

$$S = \frac{1}{eT} \mathbf{K}_1 \mathbf{K}_0^{-1}, \quad (3)$$

$$k_e = \frac{1}{T} (\mathbf{K}_2 - \mathbf{K}_1^2 \mathbf{K}_0^{-1}). \quad (4)$$

where $\tau_i(\mathbf{k})$ and ε_i are the electronic relaxation time and energy eigenvalue. k_e can be obtained based on the tensor \mathbf{K}_n .

The in-plane κ_L under relaxation time approximation can be obtained:¹²

$$\kappa_{\alpha\beta} = \frac{1}{V} \sum_{\lambda} C_{\lambda} v_{\lambda\alpha} v_{\lambda\beta} \tau_{\lambda}, \quad (5)$$

where the meaning of each parameter are explained elsewhere.¹² We use Phonopy³⁰ and ShengBTE³¹ to deal with the harmonic and anharmonic force constants. We use the equation (4) to calculate the electronic thermal conductivity k_e since sometimes the results from the Wiedemann-Franz law is unreasonable, such as in metallic VO_2 ,³² clean graphene near the charge neutral point,³³ and single-electron transistor.³⁴ As a matter of fact, the Wiedemann-Franz law is only suitable for the system where the scattering of electrons in the material is dominated by the elastic collision (“good metal”).³⁵ Therefore, we use the definition to calculate k_e . It should be noted that an effective thickness should be defined in order to calculate the electronic and thermal properties for 2D materials. The thickness of α -Te is 7.74 \AA , whose definition is clearly defined in elsewhere.^{12,36}

3 Results and discussion

The optimized structure of α -Te is shown in Figure 1a and 1b with lattice constant 4.238 Å obtained by PBE+D2 functional. The α -Te possesses $P\bar{3}M1$ (164) symmetry group belonging to trigonal system and isotropic pattern in 2D plane, which is quite different from the anisotropic bulk Te³⁷ and 2D β -Te.^{8,12} From the top and side views, α -Te and sandwiched 1T-MoS₂ look alike in many ways. Intermediate Te atom is octahedrally coordinated to six neighboring Te atoms and upper and lower Te layers form the A-B like stacking. The coordination numbers in outer and centered Te are 3 and 6, which is the characteristic of a multivalency formation of Te atom located in the near bottom of the periodic table. The bond length in α -Te is all 3.04 Å, which is larger than those of 2.77 Å and 3.03 Å (two type bonds) in monolayer β -Te.¹²

Bulk Te was reported a direct semiconductor ($E_g = 0.25$ eV)³⁷ and it also has recently been experimentally observed as a remarkable thermoelectric material.¹⁷ Figure 1c and 1d show the electronic band structure and density of states (DOS) of α -Te, indicating a near-direct band gap material ($E_g = 1.11$ eV) at HSE06 level. Our result is very consistent with the previous theoretical work.⁸

A good thermoelectric material not only needs a minimum thermal conductivity, but also requires a simultaneously maximum power factor (PF). However, Seebeck S and σ are usually interweaved. A large S requires a large carrier effective mass decided by³⁸ $S = \frac{8\pi^2 k_B^2 T}{3eh^2} m^* (\frac{\pi}{3n})^{2/3}$ in 3D semiconducting materials, but σ is inversely proportional to the carrier effective mass due to $\mu = \frac{e\tau}{m^*}$. In 1993, Hicks and Dresselhaus proposed a seminal idea that sharpen the energy dependence of the DOS in 1D and 2D systems to alleviate the coupling between S and σ , consequently enhancing the PF .^{39,40} Mahan and Sofo further generalized it to a refined sentence.⁴¹ Afterwards, these guiding principles triggered two interesting band structure shapes. One is “pudding-mold”^{42,43} and the other one is “Mexican-hat-shape”.⁴⁴ Recently, a backward thinking emerges, which introduce quasi-one-dimensional electronic band dispersions in 2D or 3D materials to increase the thermoelectric performance.^{45,46} A relatively flat band means a large DOS in a narrow energy region near

the Fermi level. The dispersive band leads to a high carrier velocity, also indicates a small m^* and therefore a high μ .⁴⁷⁻⁵⁰ Interestingly, The valence bands near the Fermi level of α -Te shown in Figure 1c has some hole pockets and relatively flat bands, which is the characteristic of a good thermoelectric property and is similar to renowned PbTe_{1-x}Se_x thermoelectrics.⁵¹

Based on the band structure, we could evaluate the S , σ , and τ of α -Te. Since the melting point of tellurium is 723 K, we select three typical temperatures (300, 500 and 700 K) in the whole calculations. Figure 2a shows the Seebeck coefficients S in the n- and p-type of α -Te as functions of carrier concentration. Overall, the absolute values of S decrease for both n- and p-type when increasing the carrier concentration, which reflects the inverse proportion between S and carrier concentration n . Moreover, the absolute value of S of hole doping is bigger than the electron doping in α -Te. For instance, the value of $|S|$ for n-type is 242.9 $\mu\text{V/K}$ at 10^{12} cm⁻² carrier concentration at 500 K temperature, only around half of p-type 529.6 $\mu\text{V/K}$ at same condition. The maximum value S of p-type α -Te is around 700 $\mu\text{V/K}$ at room temperature, which is the double of that 350 $\mu\text{V/K}$ in bulk tellurium.¹⁷ This is the physical reason that the ZT of α -Te are comparable with bulk tellurium, although the κ_L in α -Te (9.85 W/mK) is around 7 times of that in bulk tellurium (1.5 W/mK).¹⁷ In this sense, if one further increases the phonon scattering using some defects and isotope effect in α -Te, the κ_L will decrease but with the same level of Seebeck coefficient S . Then the ZT of α -Te will be significantly enhanced and surpass the bulk tellurium.¹⁷

The difference between electron and hole doping in Seebeck S originates from the electronic band structure and DOS in Figure 1c and 1d. As we discussed above, S is primarily regulated by the effect mass m^* and the magnitude of DOS. A more smooth valence band (hole-doping) compared with a conduction band (electron-doping) corresponds to a larger carrier m^* , indicating a large S since S is proportional to the m^* . Furthermore, DOS of p-type is obviously much larger than n-type of α -Te around the Fermi level shown in Figure 1d. These evidences verify that the superior performance of the hole doping compared

with the electron doping in α -Te.

According to the BTE, the electronic conductivity σ is dependent and is proportional to the relaxation time τ . Therefore, a reasonable relaxation time τ should be chosen. As a matter of fact, τ in materials is a function of temperature and carrier concentration. So far, experimental measurement may be the only effective way to solve this issue. For theoretical calculations, τ is difficult to obtain with high precision. Specifically, there are mainly three methods, such as using a designated τ based on relevant experiments,^{52,53} electro-phonon coupling implemented in EPW.⁵⁴ Another approach is based on the well-known model: $\tau = \frac{m^*\mu}{e}$ in which μ is the carrier mobility and in 2D materials using deformation potential theory acoustic phonon limited μ could be expressed as:⁵⁵

$$\mu_{2D} = \frac{e\hbar^3 C_{2D}}{k_B T m^* m_d E_i^2} \quad (6)$$

where m_d is the average effective mass dominated by $m_d = \sqrt{m_x^* m_y^*}$. E_i can be expressed as $E_i = \Delta E_i / (\Delta l / l_0)$ in which ΔE_i is the i^{th} band under small compression and expansion compared with the energy of unstrained system. Here, it supposes that the energy of core electrons, considered as the energy reference, do not change under the small deformation. This treating process is reasonable and have also been verified by the previous researches.^{45,55} The detailed calculations is shown in the Supporting Information. Our calculated effective masses m^* are $0.107 m_e$ for the conduction band minimum and $0.164 m_e$ for the valence band maximum and the carrier mobilities are $2.086 \times 10^3 \text{ cm}^2 \text{V}^{-1} \text{ s}^{-1}$ for electrons and $1.736 \times 10^3 \text{ cm}^2 \text{V}^{-1} \text{ s}^{-1}$ for holes. Our result is very consistent with the previous report.⁸ Therefore, based on $\tau = \frac{m^*\mu}{e}$, we can obtain the relaxation time of 0.127 ps for electrons and 0.163 ps for holes in α -Te.

Contrary to the Seebeck S , electronic conductivity σ increases with increasing carrier concentration. Figure 2b shows a larger σ of electron doping compared with hole doping at the same carrier concentration due to the smaller effective mass ($0.107 m_e$ for electrons $<$ $0.164 m_e$ for holes). Furthermore, σ of two type α -Te are insensitive to temperature, which is similar to that of β -Te.¹⁶

A high PF needs a large S and a large σ simultaneously. One should compromise between decreasing function of S and increasing function of σ . The calculated power factor ($S^2\sigma$) that can demonstrate the thermoelectric performance of α -Te is shown in Figure 2c. The PF for both types first increase, climb the summit at moderate carrier concentrations, and then decrease when increasing the concentration. The p-type PF is significantly larger than n-type of α -Te, though they exhibit similar trend dependent on the carrier concentration. For instance, the maximum PF of holes and electrons are 74.6 mW/mK^2 at 6.12×10^{13} concentration and 21.2 mW/mK^2 at 2.86×10^{13} concentration at 500 K. The former one is around 2.5 times larger than that of the latter one and is 2 times larger than 2D SnSe.⁵⁶

More interestingly, the maximum PF of bulk tellurium at room temperature is around 1.3 mW/mK^2 ,¹⁷ which is around a tenth of that in α -Te (12 mW/mK^2) at the similar condition shown in Figure 2c. The physical reason behind it is the very small effective mass m^* of α -Te. The m^* of standard 2H-MoS₂ is $0.47 m_e$ for electrons and $0.58 m_e$ for holes.⁸ However, in α -Te, the m^* is $0.107 m_e$ for electron and $0.164 m_e$ for holes. Obviously, the effective mass of carriers in α -Te is quite smaller than 2H-MoS₂. A smaller m^* will result in a larger electronic conductivity qualitatively decided by the simple model: $\sigma = \frac{ne^2\tau}{m^*}$. Moreover, Liu *et al.*¹⁴ pointed out that lone-pair electrons in bulk Te will significantly enhance the interchain electronic transport. Similarly, the coordination number in α -Te is 3 for outer Te atoms, which is only half of valence electrons in Te atoms (group-VI). Therefore, each outside Te atom exists 3 lone-pair electrons. These lone-pair electrons will enhance the hopping term between electrons and contribute to the superior electronic transport properties in α -Te.^{8,14}

An optimal ZT also needs a minimum thermal conductivity ($\kappa_e + \kappa_L$). For electronic thermal conductivity, k_e has been discussed in the computational methods. Next, we would like to explore the phonon transport properties of α -Te, as phonon dominates the thermal transport in semiconductors. The calculated phonon dispersions are shown in Figure 3a. Firstly, it shows that all phonon branches are free from negative and this result con-

firm the dynamical stability of α -Te. Moreover, there is no phonon gap between acoustic and optical branches, indicating a strong optical-acoustic phonon scattering which will suppress the κ_L ⁵⁷ of materials.

A high-order (≥ 3) scattering of phonons leads to a limited κ_L .^{58,59} Figure 3b shows the intrinsic κ_L computed with both non-iterative and iterative method from 100 K to 700 K. We note that both methods give similar trends of κ_L in the whole temperature range. However, the iterative method always gives values of κ_L higher than the non-iterative method at the same temperature. We choose the values of iterative method in the following discussion. We find κ_L of α -Te can be well described by the T^{-1} curve. This phenomenon is also found in bulk Te¹⁷ and β -Te.¹² The value of intrinsic κ_L is 9.85 W m⁻¹K⁻¹ (300 K), which is twice as much as that of β -Te at the same temperature.¹² Furthermore, κ_L of α -Te is also larger than bulk Te (2.77 W/mK),¹² which is consistent with the familiar trend ($\kappa_{2D} > \kappa_{3D}$).^{12,60,61}

The normalized contribution of ZA, TA, LA and optical branches varying with temperature are plotted in Figure 3c, in which each mode varies small at different temperatures especially beyond 200 K, and can be regarded as independent of temperature, similar with the β -Te.¹² At room temperature, three acoustic branches contribute about 90% to the total intrinsic κ_L , while the summation of all optical phonons is only 10%. Furthermore, the proportions of contributions to total κ_L are about 25%, 47%, and 17% for LA, TA, and ZA phonons, in which ZA mode is the smallest one among three acoustic branches in α -Te, quite different from graphene where the proportion of ZA mode is about 75%.⁶²

It was reported that there is a symmetry selection rule in flat graphene that only even number of ZA modes can be involved in scattering processes.^{63,64} This rule originates from the reflection symmetry about c axis in the structure. The thermal resistance roots in the high order of phonon scattering. Due to the selection rule, ZA mode contributes mainly to the κ in graphene. However, the lattice does not have the reflection symmetry about c axis in α -Te. As a result the selection rule is broken, the importance of ZA mode in thermal transport of α -Te is much smaller than graphene.

Moreover, it is worthwhile to explore the contribution of phonons with different frequencies to the total κ_L . Here the frequency-resolved κ_L for α -Te at 300 K is displayed in Figure 3d. It can be found that the main contribution originates from acoustic phonons with frequencies lower than 2 THz, while the contribution of optical phonons is very small. This is consistent with Figure 3c. Furthermore, the acoustic phonons with very low frequency (lower than 1 THz) contribute most to κ_L . In the following, we will find the behind reason is that phonons around Γ point usually possess large phonon relaxation time.

All samples of material have finite size in practical experiment and device application, thus the additional boundary scattering will reduce κ_L , especially at nanoscale or at low temperatures. Usually, in nanostructures, κ_L related to boundary scattering can be evaluated as:^{12,61}

$$\frac{1}{\tau_\lambda^B} = \frac{v_\lambda}{L}, \quad (7)$$

where L is the size of material. This formula represents the situation for a completely diffusive boundary scattering of phonons. Cumulative κ_L ($\wedge < \wedge_{max}$) can also be used to study the size effect, whose definition has been defined elsewhere.³¹ Figure 3e shows the size dependence of κ_L for α -Te with completely diffusive boundary scattering at room temperature and the cumulative κ_L is displayed in Figure 3f. In Figure 3e, κ_L becomes lower while the sample size getting smaller, as the boundary scattering becomes larger. For a specific example, when the sample size is 1 μ m, κ_L can be suppressed to 7.56 W m⁻¹K⁻¹, about 78% of value for the infinitely large system. When the sample size is 10 μ m, κ_L reaches 91% of the infinitely large system. It implies the size effect always keeps till about 10 μ m, such as 2D WTe₂.⁶⁵

The size effect can also be estimated from the cumulative κ_L as a function of MFP shown in Figure 3f. We can find that the MFP range of phonons that contribute significantly to κ_L is about 10 nm to 10 μ m, which is consistent with our previous result in Figure 3e. In order to obtain the representative MFP, we fit cumulative κ_L using a single parametric function: $\kappa(\wedge \leq \wedge_{max}) = \kappa_{max}/(1 + \wedge_0/\wedge_{max})$, where κ_{max} is κ_L of infinite size, \wedge_{max}

is the maximal MFP. The fitting parameter Λ_0 can be interpreted as the typical MFP with which the phonons contribute significantly to κ_L . The fitted curve is shown in Figure 3f by dashed line. The parameter Λ_0 is 94 nm, which could be interpreted as the representative MFP of α -Te. This implies the κ_L of α -Te may decline sharply with the sample size of hundreds of nm. This property is propitious to the electronic and thermoelectric materials based on α -Te in the nanoscale.¹⁰

Group velocity of phonon has great effects on thermal transport of materials, as it is proportional to v^2 based on Eq. (3). The calculated v^2 with different frequencies are shown in Figure 4a. LA branch possesses the highest v among three acoustic branches, specifically more than two times of that for ZA and TA phonons. The optical phonons around 3.7 THz has the largest v but they only contribute 10% to total κ_L . Here τ is also displayed in Figure 4b. τ around Γ point has the magnitude of 10^3 - 10^4 ps but τ of most phonons with frequency more than 5 THz is about 0.1-10 ps. That is the reason why phonons with very low frequency dominate the thermal transport in α -Te (Figure 3d). Furthermore, τ of TA branch is the largest of all, about 10^4 ps around the Γ point. That is the reason why TA mode contributes most to κ_L even more than LA phonons (Figure 3c). It can also explain that optical phonons contribute little to κ_L since most of them have ultralow τ of only 1 to 10 ps.

Grünerisen parameter provides crucial information on the anharmonic interactions of phonons. γ in α -Te for whole frequency spectrum is displayed in Figure 4c. γ of TA and LA modes are in the range of 0-2, while those of optical modes are 1-6. Comparing with β -Te, γ of α -Te are smaller, indicating a lower anharmonicity and a higher κ_L .¹² Interestingly, it can be found γ of acoustic and optical phonon modes have suddenly dropped around 2-2.5 THz. Since there is no acoustic-optical phonon gap, the large acoustic-optical phonon scattering would lead to a giant γ and is also the source of ultralow κ_L in β -Te.¹² In the three-phonon scattering process, all phonon modes must be satisfied the conservation of energy and momentum simultaneously.⁶⁶ The quantitative probability of all available three-phonon scattering in α -Te are shown in Figure 4d. This

P_3 phase space is one order smaller than of β -Te, indicating a weaker anharmonicity of α -Te compared with β -Te.¹²

Based on the above results, intrinsic figure of merit ZT can be evaluated and exhibited in Figure 5. The climax ZT at 700 K are 0.57 and 0.83 for electron and hole doping α -Te, which is as high as β -Te¹⁶ and has the same order of bulk Te.¹⁷ Room temperature ZT of n-type α -Te is 0.54. Our calculation suggests that monolayer α -Te is a promising thermoelectric material. Furthermore, it can be promoted further via suppressing κ_L such as grain boundary, isotope effect and vacancy.⁶⁷

4 Conclusion

In summary, we have systematically studied the extraordinarily high thermoelectric performance of monolayer α -Te by the *ab initio* calculations. To explain the high ZT , we consider the electronic and thermal transport properties. A large and asymmetric electronic density of states induce relatively flat bands, leading to a large Seebeck coefficient S . A small effective carrier mass m^* of CBM (VBM) will result in a larger electronic conductivity σ . Combining both, the PF in α -Te (12 mW/mK^2) exhibits ten times as large as that in bulk tellurium (1.3 mW/mK^2)¹⁷ at the similar condition. For lattice thermal conductivity κ_L , α -Te consists of heavy atomic mass, which breeds low harmonic properties, such as low group velocities. For anharmonicity, strong phonon anharmonic scattering rates including acoustic-optical phonon scattering bring about a same order of magnitude κ_L of α -Te compared with the bulk Te and β -Te. A superior electronic properties and a suitable κ_L combine together leading to the ultrahigh ZT in α -Te. A maximum ZT of 0.83 is achieved with reasonable hole concentration at 700 K. Our results indicate that monolayer α -Te is a promising thermoelectric material. We hope that α -Te, more stable than β -Te, would be experimentally observed with high ZT in the near future.

5 Supporting Information

The Supporting Information is available free of charge on the ACS Publications website via the Internet at <https://pubs.acs.org/journal/aamick>.

Electronic band structure and effective mass around conduction band minimum and valence band maximum of two-dimensional tellurium.

Author Information

Corresponding Author

*E-mail: liugang8105@gmail.com

*E-mail: Xonics@tongji.edu.cn

ORCID

Zhibin Gao: 0000-0002-6843-381X

Jie Ren: 0000-0003-2806-7226

Notes

The authors declare no competing financial interest.

Acknowledgement We thank our member Yi Wang for helpful discussions. This work is supported by the National Natural Science Foundation of China (No. 11775159), the Natural Science Foundation of Shanghai (No. 18ZR1442800), the National Youth 1000 Talents Program in China, and the Opening Project of Shanghai Key Laboratory of Special Artificial Microstructure Materials and Technology. Computational resources have been provided by the Tongji University.

References

- (1) Novoselov, K. S.; Geim, A. K.; Morozov, S. V.; Jiang, D.; Zhang, Y.; Dubonos, S. V.; Grigorieva, I. V.; Firsov, A. A. Electric Field Effect in Atomically Thin Carbon Films. *Science* **2004**, *306*, 666–669.
- (2) Mounet, N.; Gibertini, M.; Schwaller, P.; Campi, D.; Merkys, A.; Marrazzo, A.; Sohler, T.; Castelli, I. E.; Cepellotti, A.; Pizzi, G.; Marzari, N. Two-Dimensional Materials from High-Throughput Computational Exfoliation of Experimentally Known Compounds. *Nat. Nanotechnol.* **2018**, *13*, 246.
- (3) Dresselhaus, M. S.; Chen, G.; Tang, M. Y.; Yang, R.; Lee, H.; Wang, D.; Ren, Z.; Fleurial, J.-P.; Gogna, P. New Directions for Low-Dimensional Thermoelectric Materials. *Adv. Mater.* **2007**, *19*, 1043–1053.
- (4) Tang, H.; Ismail-Beigi, S. Novel Precursors for Boron Nanotubes: The Competition of Two-Center and Three-Center Bonding in Boron Sheets. *Phys. Rev. Lett.* **2007**, *99*, 115501.
- (5) Li, D.; He, J.; Ding, G.; Tang, Q.; Ying, Y.; He, J.; Zhong, C.; Liu, Y.; Feng, C.; Sun, Q.; Zhou, H.; ; Zhou, P.; Zhang, G. Stretch-Driven Increase in Ultrahigh Thermal Conductance of Hydrogenated Borophene and Dimensionality Crossover in Phonon Transmission. *Adv. Funct. Mater.* **2018**, *28*, 1801685.
- (6) Guan, J.; Zhu, Z.; Tománek, D. Phase Coexistence and Metal-Insulator Transition in Few-Layer Phosphorene: A Computational Study. *Phys. Rev. Lett.* **2014**, *113*, 046804.
- (7) Li, L.; Yu, Y.; Ye, G. J.; Ge, Q.; Ou, X.; Wu, H.; Feng, D.; Chen, X. H.; Zhang, Y. Black Phosphorus Field-Effect Transistors. *Nat. Nanotechnol.* **2014**, *9*, 372.
- (8) Zhu, Z.; Cai, X.; Yi, S.; Chen, J.; Dai, Y.; Niu, C.; Guo, Z.; Xie, M.; Liu, F.; Cho, J.-H.;

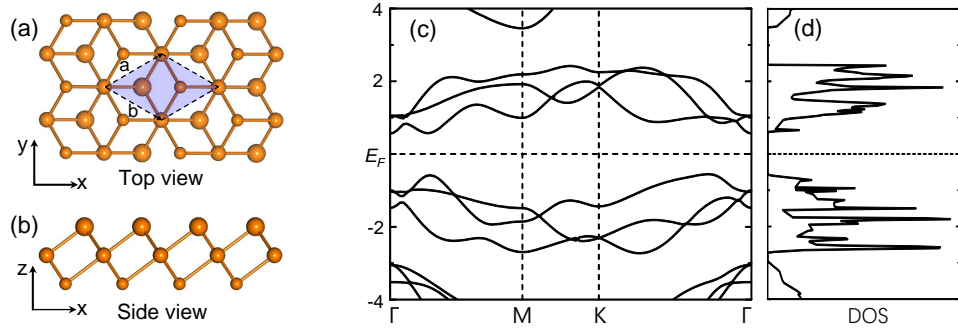


Figure 1: (a)(b) Top and side views of the optimized α -Te monolayer structure. The primitive cell is indicated by the blue shading in the top view. a and b are the lattice vectors spanning the 2D lattice. (c)(d) Electronic band structure and density of states (DOS) of α -Te at HSE06 level. The Fermi levels are set to zero.

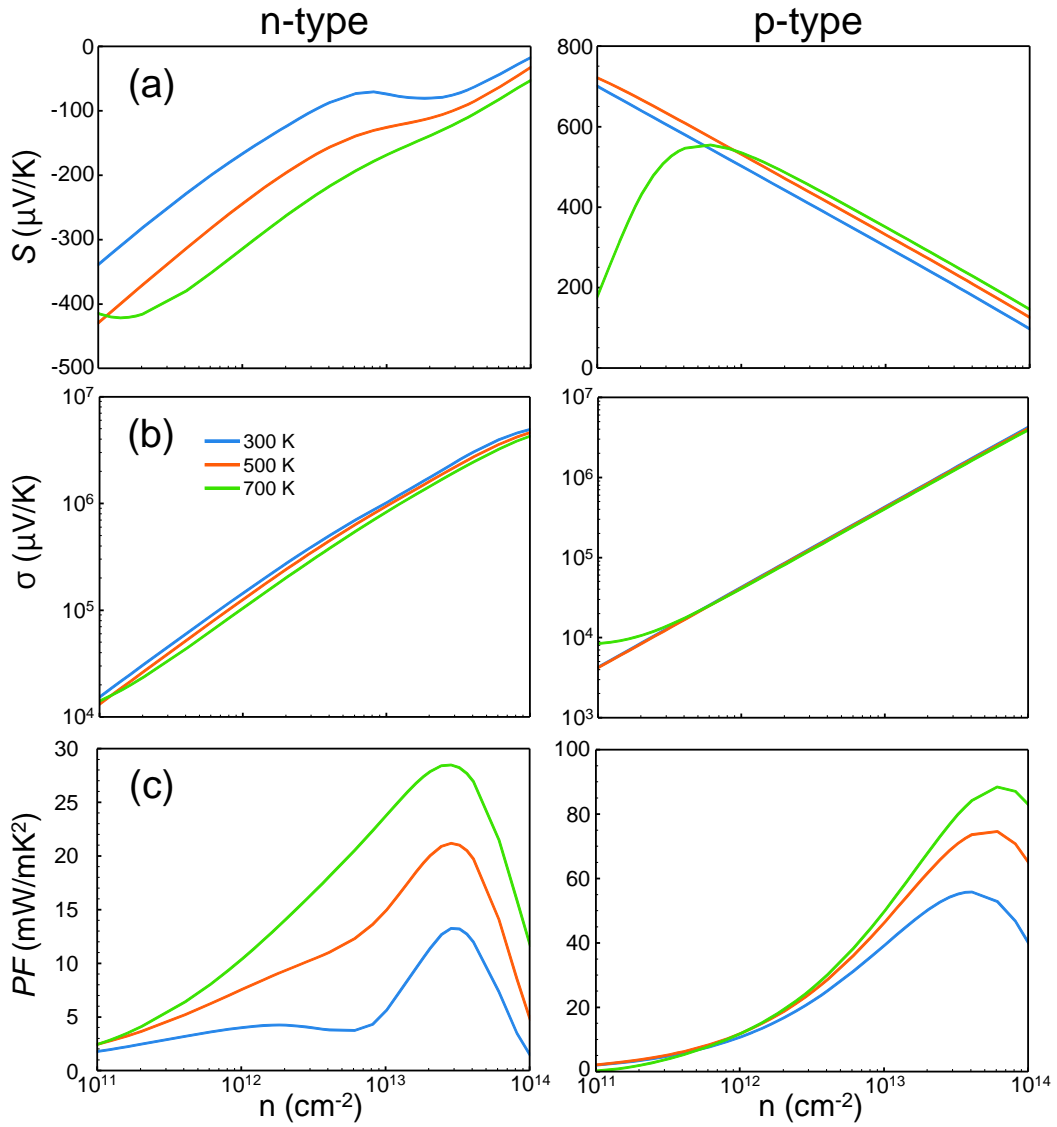


Figure 2: Temperature-dependent electronic transport coefficients. (a) Seebeck coefficient, (b) electrical conductivity, and (c) power factor ($S^2\sigma$) of the α -Te as a function of carrier concentration along a or b axis at 300, 500, and 700 K.

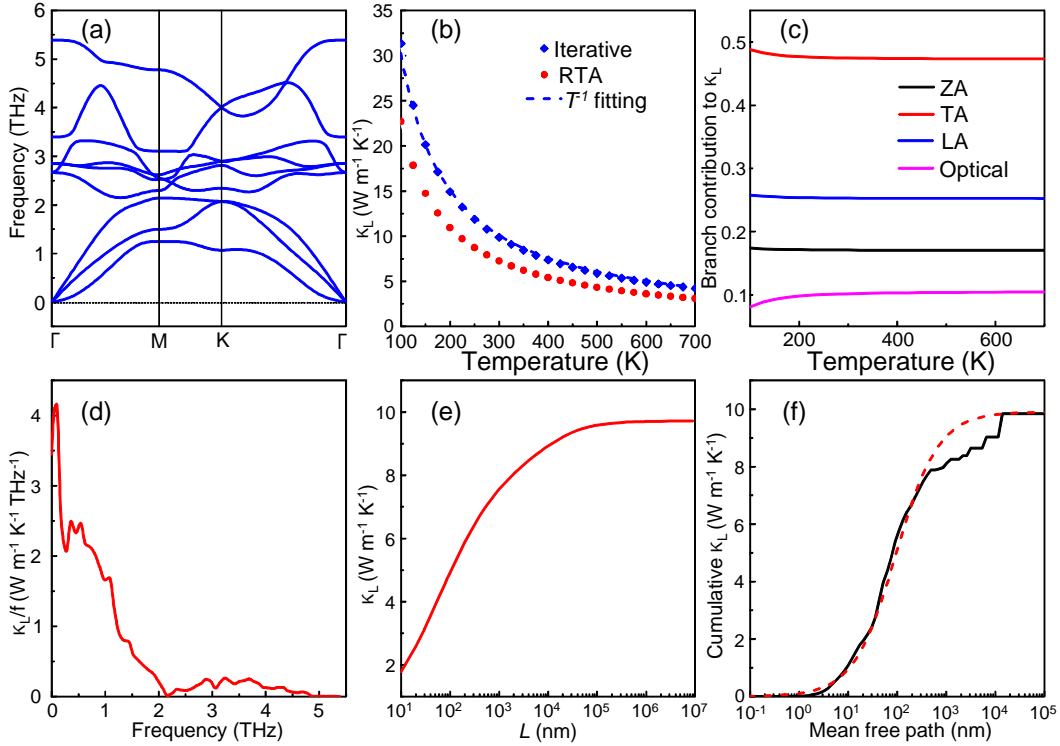


Figure 3: (a) Phonon spectra and DOS of α -Te. (b) Intrinsic lattice thermal conductivity κ_L as a function of temperature. Blue dashed line is T^{-1} fitting. The values of relaxation time approximation (RTA) are also shown by red dots. (c) Normalized contributions to total κ_L of phonon branches from 100 to 700 K. (d) Frequency-resolved κ_L at room temperature. (e) Room-temperature κ_L as a function of sample size. (f) Cumulative κ_L as a function of phonon mean free path (MFP) at room temperature. The fitted curve is plotted in a dashed line.

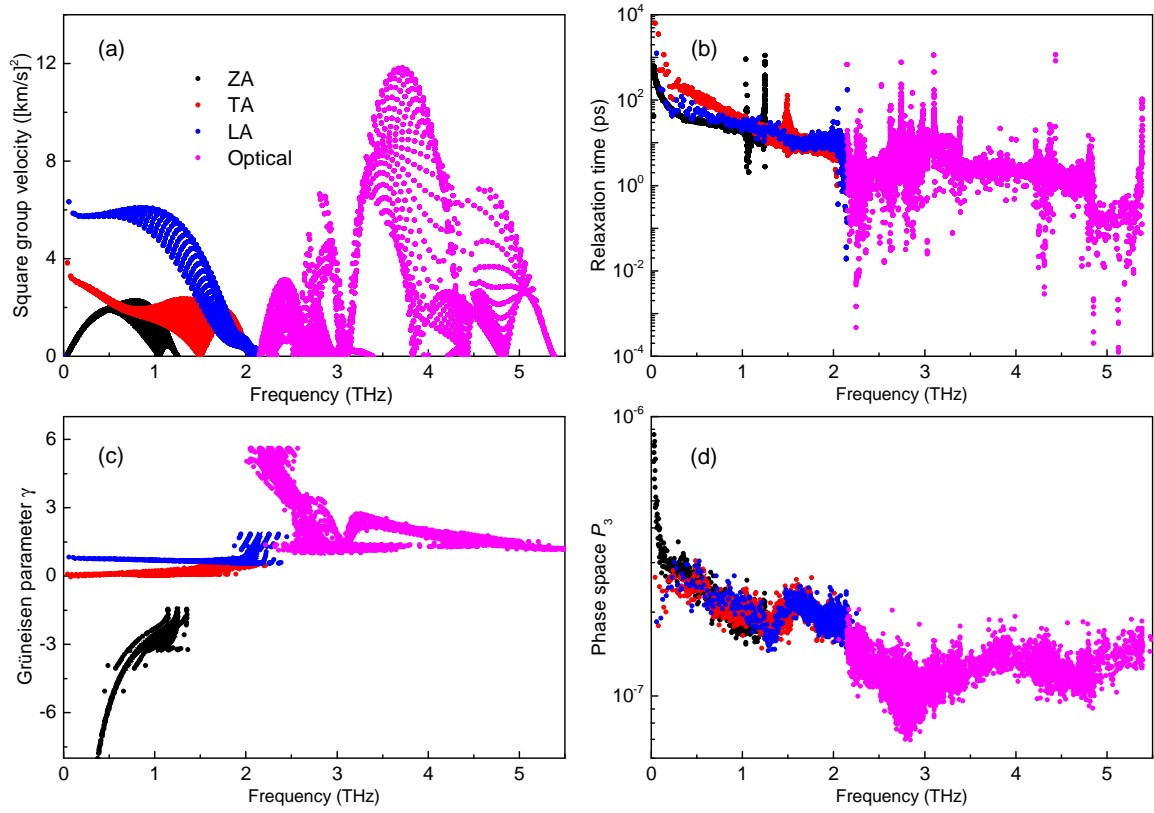


Figure 4: (a) The frequency dependent behavior of square group velocity at 300 K for α -Te. All optical phonon branches are in purple. (b) Phonon relaxation time of ZA, TA, LA, and optical phonon branches as a function of frequency at room temperature. (c) Mode-Grüneisen parameter and (d) Phase-space volume P_3 for three-phonon scattering processes.

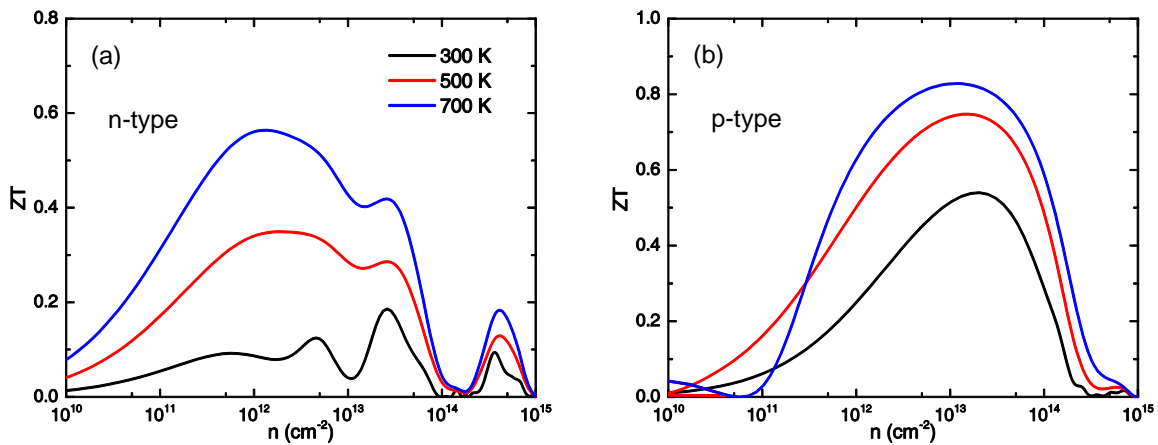


Figure 5: Calculated (a) n-type and (b) p-type ZT values of monolayer α -Te as a function of carrier concentration along a or b axis at 300, 500 and 700 K.

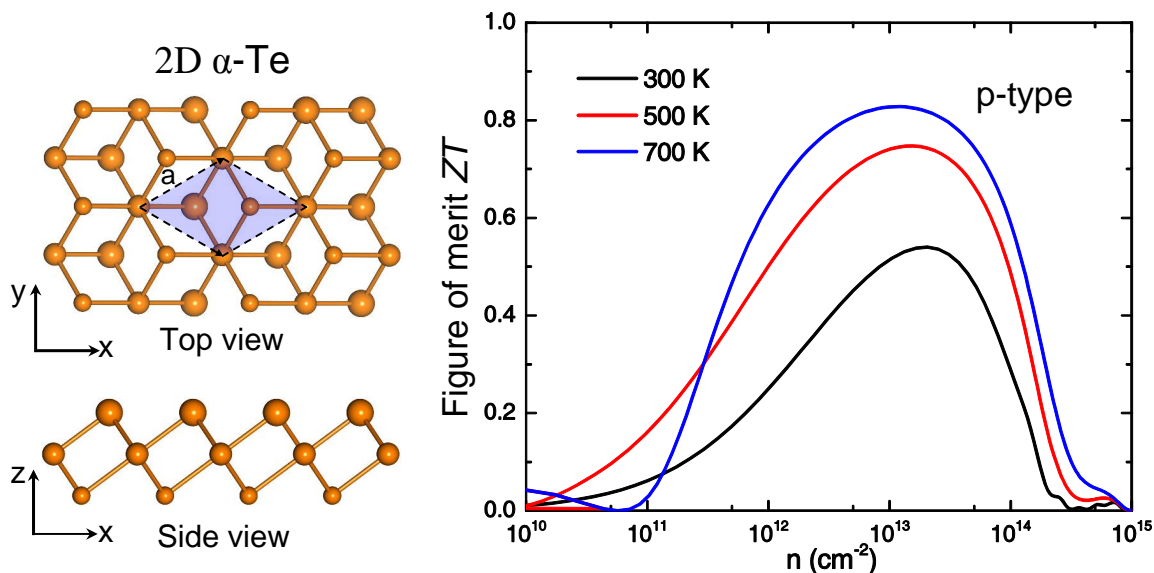


Table of Contents Graphic

- Jia, Y.; Zhang, Z. Multivalency-Driven Formation of Te-Based Monolayer Materials: A Combined First-Principles and Experimental Study. *Phys. Rev. Lett.* **2017**, *119*, 106101.
- (9) Huang, X.; Guan, J.; Lin, Z.; Liu, B.; Xing, S.; Wang, W.; Guo, J. Epitaxial Growth and Band Structure of Te Film on Graphene. *Nano Lett.* **2017**, *17*, 4619–4623.
- (10) Wang, Y.; Qiu, G.; Wang, R.; Huang, S.; Wang, Q.; Liu, Y.; Du, Y.; Goddard, W. A.; Kim, M. J.; Xu, X.; Ye, P. D.; Wu, W. Field-Effect Transistors Made from Solution-Grown Two-Dimensional Tellurene. *Nat. Electron.* **2018**, *1*, 228.
- (11) Du, Y.; Qiu, G.; Wang, Y.; Si, M.; Xu, X.; Wu, W.; Ye, P. D. One-Dimensional Van der Waals Material Tellurium: Raman Spectroscopy under Strain and Magneto-Transport. *Nano Lett.* **2017**, *17*, 3965–3973.
- (12) Gao, Z.; Tao, F.; Ren, J. Unusually Low Thermal Conductivity of Atomically Thin 2D Tellurium. *Nanoscale* **2018**, *10*, 12997–13003.
- (13) Chen, J.; Dai, Y.; Ma, Y.; Dai, X.; Ho, W.; Xie, M. Ultrathin β -Tellurium Layers Grown on Highly Oriented Pyrolytic Graphite by Molecular-Beam Epitaxy. *Nanoscale* **2017**, *9*, 15945–15948.
- (14) Liu, Y.; Wu, W.; Goddard, W. A. Tellurium: Fast Electrical and Atomic Transport Along the Weak Interaction Direction. *J. Am. Chem. Soc.* **2018**, *140*, 550–553.
- (15) Qiao, J.; Pan, Y.; Yang, F.; Wang, C.; Chai, Y.; Ji, W. Few-layer Tellurium: One-Dimensional-Like Layered Elementary Semiconductor with Striking Physical Properties. *Sci. Bull.* **2018**, *63*, 159 – 168.
- (16) Sharma, S.; Singh, N.; Schwingenschlögl, U. Two-Dimensional Tellurene as Excellent Thermoelectric Material. *ACS Appl. Energy Mater.* **2018**, *1*, 1950–1954.
- (17) Lin, S.; Li, W.; Chen, Z.; Shen, J.; Ge, B.; Pei, Y. Tellurium as a High-Performance Elemental Thermoelectric. *Nat. Commun.* **2016**, *7*, 10287.
- (18) Lee, S.; Esfarjani, K.; Luo, T.; Zhou, J.; Tian, Z.; Chen, G. Resonant Bonding Leads to Low Lattice Thermal Conductivity. *Nat. Commun.* **2014**, *5*, 3525.
- (19) Tadano, T.; Gohda, Y.; Tsuneyuki, S. Impact of Rattlers on Thermal Conductivity of a

- Thermoelectric Clathrate: A First-Principles Study. *Phys. Rev. Lett.* **2015**, *114*, 095501.
- (20) Jana, M. K.; Pal, K.; Waghmare, U. V.; Biswas, K. The Origin of Ultralow Thermal Conductivity in InTe: Lone-Pair-Induced Anharmonic Rattling. *Angew. Chem., Int. Ed.* **2016**, *128*, 7923–7927.
- (21) Snyder, G. J.; Toberer, E. S. Complex Thermoelectric Materials. *Nat. Mater.* **2008**, *7*, 105–114.
- (22) Liu, H.; Shi, X.; Xu, F.; Zhang, L.; Zhang, W.; Chen, L.; Li, Q.; Uher, C.; Day, T.; Snyder, G. J. Copper Ion Liquid-Like Thermoelectrics. *Nat. Mater.* **2012**, *11*, 422.
- (23) Blöchl, P. E. Projector Augmented-Wave Method. *Phys. Rev. B: Condens. Matter Mater. Phys.* **1994**, *50*, 17953–17979.
- (24) Kresse, G.; Joubert, D. From ultrasoft pseudopotentials to the projector augmented-wave method. *Phys. Rev. B: Condens. Matter Mater. Phys.* **1999**, *59*, 1758–1775.
- (25) Perdew, J. P.; Burke, K.; Ernzerhof, M. Generalized Gradient Approximation Made Simple. *Phys. Rev. Lett.* **1996**, *77*, 3865–3868.
- (26) Heyd, J.; Scuseria, G. E.; Ernzerhof, M. Hybrid functionals based on a screened Coulomb potential. *J. Chem. Phys.* **2003**, *118*, 8207–8215.
- (27) Grimme, S. Semiempirical GGA-Type Density Functional Constructed with a Long-Range Dispersion Correction. *J. Comput. Chem.* **2006**, *27*, 1787–1799.
- (28) Madsen, G. K.; Singh, D. J. BoltzTraP. A code for calculating band-structure dependent quantities. *Comput. Phys. Commun.* **2006**, *175*, 67–71.
- (29) Chen, M. X.; Podloucky, R. Electronic thermal conductivity as derived by density functional theory. *Phys. Rev. B: Condens. Matter Mater. Phys.* **2013**, *88*, 045134.
- (30) Togo, A.; Oba, F.; Tanaka, I. First-Principles Calculations of the Ferroelastic Transition Between Rutile-Type and CaCl₂-Type SiO₂ at High Pressures. *Phys. Rev. B: Condens. Matter Mater. Phys.* **2008**, *78*, 134106.
- (31) Li, W.; Carrete, J.; Katcho, N. A.; Mingo, N. ShengBTE: A Solver of the Boltzmann Transport Equation for Phonons. *Comput. Phys. Commun.* **2014**, *185*, 1747.
- (32) Lee, S.; Hippalgaonkar, K.; Yang, F.; Hong, J.; Ko, C.; Suh, J.; Liu, K.; Wang, K.; Urban, J. J.; Zhang, X.; Dames, C.; Hartnoll, S. A.; Delaire, O.; Wu, J. Anomalous Low Electronic Thermal Conductivity in Metallic Vanadium Dioxide. *Science* **2017**, *355*, 371–374.
- (33) Crossno, J.; Shi, J. K.; Wang, K.; Liu, X.; Harzheim, A.; Lucas, A.; Sachdev, S.; Kim, P.; Taniguchi, T.; Watanabe, K.; Ohki, T. A.; Fong, K. C. Observation of the Dirac fluid and the breakdown of the Wiedemann-Franz law in graphene. *Science* **2016**, *351*, 1058–1061.
- (34) Dutta, B.; Peltonen, J. T.; Antonenko, D. S.; Meschke, M.; Skvortsov, M. A.; Kubala, B.; König, J.; Winkelmann, C. B.; Courtois, H.; Pekola, J. P. Thermal conductance of a single-electron transistor. *Phys. Rev. Lett.* **2017**, *119*, 077701.
- (35) Mosso, N.; Drechsler, U.; Menges, F.; Nirmalraj, P.; Karg, S.; Riel, H.; Gotsmann, B. Heat transport through atomic contacts. *Nat. Nanotechnol.* **2017**, *12*, 430.
- (36) Gao, Z.; Dong, X.; Li, N.; Ren, J. Novel two-dimensional silicon dioxide with in-plane negative Poisson's ratio. *Nano Lett.* **2017**, *17*, 772–777.
- (37) Peng, H.; Kioussis, N.; Snyder, G. J. Elemental tellurium as a chiral *p*-type thermoelectric material. *Phys. Rev. B: Condens. Matter Mater. Phys.* **2014**, *89*, 195206.
- (38) Heremans, J. P.; Jovovic, V.; Toberer, E. S.; Saramat, A.; Kurosaki, K.; Charoenphakdee, A.; Yamanaka, S.; Snyder, G. J. En-

hancement of Thermoelectric Efficiency in PbTe by Distortion of the Electronic Density of States. *Science* **2008**, *321*, 554–557.

- (39) Hicks, L. D.; Dresselhaus, M. S. Effect of Quantum-Well Structures on the Thermoelectric Figure of Merit. *Phys. Rev. B: Condens. Matter Mater. Phys.* **1993**, *47*, 12727–12731.
- (40) Hicks, L. D.; Dresselhaus, M. S. Thermoelectric Figure of Merit of a One-Dimensional Conductor. *Phys. Rev. B: Condens. Matter Mater. Phys.* **1993**, *47*, 16631–16634.
- (41) Mahan, G. D.; Sofo, J. O. The Best Thermoelectric. *Proc. Natl. Acad. Sci. U. S. A.* **1996**, *93*, 7436–7439.
- (42) Kuroki, K.; Arita, R. “Pudding Mold” Band Drives Large Thermopower in Na_xCoO_2 . *J. Phys. Soc. Jpn.* **2007**, *76*, 083707.
- (43) Usui, H.; Suzuki, K.; Kuroki, K.; Nakano, S.; Kudo, K.; Nohara, M. Large Seebeck Effect in Electron-Doped FeAs_2 Driven by a Quasi-One-Dimensional Pudding-Mold-Type Band. *Phys. Rev. B: Condens. Matter Mater. Phys.* **2013**, *88*, 075140.
- (44) Ge, X.-J.; Qin, D.; Yao, K.-L.; Lü, J.-T. First-Principles Study of Thermoelectric Transport Properties of Monolayer Gallium Chalcogenides. *J. Phys. D, Appl. Phys.* **2017**, *50*, 405301.
- (45) Mi, X.-Y.; Yu, X.; Yao, K.-L.; Huang, X.; Yang, N.; L, J.-T. Enhancing the Thermoelectric Figure of Merit by Low-Dimensional Electrical Transport in Phonon-Glass Crystals. *Nano Lett.* **2015**, *15*, 5229–5234.
- (46) Bilc, D. I.; Hautier, G.; Waroquiers, D.; Rignanese, G.-M.; Ghosez, P. Low-Dimensional Transport and Large Thermoelectric Power Factors in Bulk Semiconductors by Band Engineering of Highly Directional Electronic States. *Phys. Rev. Lett.* **2015**, *114*, 136601.
- (47) Yang, J.; Liu, R.; Chen, Z.; Xi, L.; Yang, J.; Zhang, W.; Chen, L. Power Factor Enhancement in Light Valence Band p -Type Skutterudites. *Appl. Phys. Lett.* **2012**, *101*, 022101.
- (48) Yang, J.; Qiu, P.; Liu, R.; Xi, L.; Zheng, S.; Zhang, W.; Chen, L.; Singh, D. J.; Yang, J. Trends in Electrical Transport of p -Type Skutterudites $R\text{Fe}_4\text{Sb}_{12}$ ($R = \text{Na, K, Ca, Sr, Ba, La, Ce, Pr, Yb}$) from First-Principles Calculations and Boltzmann Transport Theory. *Phys. Rev. B: Condens. Matter Mater. Phys.* **2011**, *84*, 235205.
- (49) Yang, J.; Li, H.; Wu, T.; Zhang, W.; Chen, L.; Yang, J. Evaluation of Half-Heusler Compounds as Thermoelectric Materials Based on the Calculated Electrical Transport Properties. *Adv. Funct. Mater.* **2008**, *18*, 2880–2888.
- (50) Yang, J.; Xi, L.; Qiu, W.; Wu, L.; Shi, X.; Chen, L.; Yang, J.; Zhang, W.; Uher, C.; Singh, D. J. On the Tuning of Electrical and Thermal Transport in Thermoelectrics: an Integrated Theory–Experiment Perspective. *NPJ. Comput. Mater.* **2016**, *2*, 15015.
- (51) Pei, Y.; Shi, X.; LaLonde, A.; Wang, H.; Chen, L.; Snyder, G. J. Convergence of Electronic Bands for High Performance Bulk Thermoelectrics. *Nature* **2011**, *473*, 66.
- (52) Bilc, D. I.; Hautier, G.; Waroquiers, D.; Rignanese, G.-M.; Ghosez, P. Low-Dimensional Transport and Large Thermoelectric Power Factors in Bulk Semiconductors by Band Engineering of Highly Directional Electronic States. *Phys. Rev. Lett.* **2015**, *114*, 136601.
- (53) He, J.; Amsler, M.; Xia, Y.; Naghavi, S. S.; Hegde, V. I.; Hao, S.; Goedecker, S.; Ozoliņš, V.; Wolverton, C. Ultralow Thermal Conductivity in Full Heusler Semiconductors. *Phys. Rev. Lett.* **2016**, *117*, 046602.
- (54) Poncé, S.; Margine, E.; Verdi, C.; Giustino, F. EPW: Electron–phonon Coupling, Transport and Superconducting Properties Using Maximally Localized Wannier Functions. *Comput. Phys. Commun.* **2016**, *209*, 116–133.

- (55) Qiao, J.; Kong, X.; Hu, Z.-X.; Yang, F.; Ji, W. High-Mobility Transport Anisotropy and Linear Dichroism in Few-Layer Black Phosphorus. *Nat. Commun.* **2014**, *5*, 4475.
- (56) Wang, F. Q.; Zhang, S.; Yu, J.; Wang, Q. Thermoelectric Properties of Single-Layered SnSe Sheet. *Nanoscale* **2015**, *7*, 15962–15970.
- (57) Lindsay, L.; Broido, D. A.; Reinecke, T. L. First-Principles Determination of Ultrahigh Thermal Conductivity of Boron Arsenide: A Competitor for Diamond? *Phys. Rev. Lett.* **2013**, *111*, 025901.
- (58) Gao, Z.; Li, N.; Li, B. Heat Conduction and Energy Diffusion in Momentum-Conserving One-Dimensional Full-Lattice Ding-a-Ling Model. *Phys. Rev. E* **2016**, *93*, 022102.
- (59) Gao, Z.; Li, N.; Li, B. Stretch Diffusion and Heat Conduction in One-Dimensional Nonlinear Lattices. *Phys. Rev. E* **2016**, *93*, 032130.
- (60) Seol, J. H.; Jo, I.; Moore, A. L.; Lindsay, L.; Aitken, Z. H.; Pettes, M. T.; Li, X.; Yao, Z.; Huang, R.; Broido, D.; Mingo, N.; Ruoff, R. S.; Shi, L. Two-Dimensional Phonon Transport in Supported Graphene. *Science* **2010**, *328*, 213–216.
- (61) Balandin, A. A. Thermal Properties of Graphene and Nanostructured Carbon Materials. *Nat. Mater.* **2011**, *10*, 569–581.
- (62) Lindsay, L.; Li, W.; Carrete, J.; Mingo, N.; Broido, D. A.; Reinecke, T. L. Phonon Thermal Transport in Strained and Unstrained Graphene from First Principles. *Phys. Rev. B: Condens. Matter Mater. Phys.* **2014**, *89*, 155426.
- (63) Lindsay, L.; Broido, D. A.; Mingo, N. Flexural Phonons and Thermal Transport in Graphene. *Phys. Rev. B: Condens. Matter Mater. Phys.* **2010**, *82*, 115427.
- (64) Peng, B.; Zhang, H.; Shao, H.; Xu, Y.; Ni, G.; Zhang, R.; Zhu, H. Phonon Transport Properties of Two-Dimensional Group-IV Materials from *ab initio* Calculations. *Phys. Rev. B: Condens. Matter Mater. Phys.* **2016**, *94*, 245420.
- (65) Ma, J.; Chen, Y.; Han, Z.; Li, W. Strong Anisotropic Thermal Conductivity of Monolayer WTe₂. *2D Mater.* **2016**, *3*, 045010.
- (66) Lindsay, L.; Broido, D. Three-Phonon Phase Space and Lattice Thermal Conductivity in Semiconductors. *Journal of Physics: Condensed Matter* **2008**, *20*, 165209.
- (67) Lv, B.; Lan, Y.; Wang, X.; Zhang, Q.; Hu, Y.; Jacobson, A. J.; Broido, D.; Chen, G.; Ren, Z.; Chu, C.-W. Experimental Study of the Proposed Super-Thermal-Conductor: BAs. *Appl. Phys. Lett.* **2015**, *106*, 074105.